
Article:
Shaikh, Moniruzzaman, Jana, Kamalesh, Lad, Amit D. et al. (2018) Tracking ultrafast dynamics of intense shock generation and breakout at target rear. Physics of Plasmas. ISSN: 1089-7674

https://doi.org/10.1063/1.5049815

Tracking ultrafast dynamics of intense shock generation and breakout at target rear

Moniruzzaman Shaikh,[1] Kamalesh Jana,[1] Amit D. Lad,[1] Indranuj Dey,[1] Sudipta. L. Roy,[1] Deep Sarkar,[1] Yash M. Ved,[1] Alex P. L. Robinson,[2] John Pasley,[3] and G. Ravindra Kumar[1,*]

[1] *Tata Institute of Fundamental Research, 1 Homi Bhabha Road, Mumbai 400005, India*
[2] *Central Laser Facility, Rutherford-Appleton Laboratory, Chilton, Didcot OX11 0QX, United Kingdom*
[3] *York Plasma Institute, University of York, Heslington, York YO10 5DQ, United Kingdom*

We report upon the picosecond plasma dynamics at the rear surface of a thin aluminium foil (of either 5.5 μm or 12μm thickness) excited by high contrast (picosecond intensity contrast of 10^{-10}), 800 nm, femtosecond pulses at an intensity of 3×10^{19} W/cm^2. We employ ultrafast pump-probe reflectometry using a second harmonic probe (400 nm) interacting with the rear surface of the target. A rise in the probe reflectivity 30 picoseconds after the pump pulse interaction reveals the breakout of a shock wave at the target rear surface which reflects the 400 nm probe pulse. Simulations using the ZEPHYROS hybrid particle-in-cell code were performed to understand the heating of the target under the influence of the high intensity laser pulse, and the temperature profile was then passed to the radiation-hydrodynamics simulation code HYADES in order to model the shock wave propagation in the target. A good agreement was found between the calculations and experimental results.

INTRODUCTION

High intensity, femtosecond laser pulses can create 'extreme' states of matter on a table-top. The plasma that such lasers are able to create upon interaction with a solid surface can have a high energy-density and can be employed to gain insights into a range of astrophysical pheneomena [1, 2]. Understanding the basic properties of this hot and dense plasma is important for basic plasma physics [2], high energy density science in general [3] and applications ranging from ICF [4] to table-top particle accelerators [5]. The dynamics of this phase are quite complex as the target interior is energised by laser-driven fast electrons and shock waves. Recent pump-probe Doppler spectrometry measurements have shown that an inward moving shock can travel through the plasma [6–8]. Hydrodynamic behaviour at the rear of the target can encompass a number of distinct behaviours. Prompt heating by fast electrons can result in rapid rarefaction of the target rear surface. Shock waves can propagate from the front surface to the rear, or alternatively shock waves may be formed at depth in the target due to the temperature gradients set up by the hot electron driven heating. The hydrodynamic behaviour at the target rear, whether driven by prompt heating and rarefaction, or by shock acceleration, can modify the sheath potential at the target-vacuum interface thereby influencing the ion acceleration that occurs there. Complete characterization of this rear-surface plasma is therefore required in order to understand the dynamics of particle acceleration. Pump-probe reflectometry is a powerful tool in understanding the plasma dynamics [8, 9]. Probing the plasma at the front of the target has helped in the understanding of the motion of the critical density surface [6–8] and revealed a novel hydrodynamic phenomenon that generates terahertz acoustic waves [10]. Several studies [11–14] deal with high-intensity short-pulse laser-driven hot-electron-induced shock-wave generation and propagation on longer time scales (>10 ps). Whereas, few studies [15–17] measure plasma dynamics at the target rear-surface on ultrashort timescales.

In this article, we consider the temporal evolution of the plasma reflectivity of the rear surface of an aluminium foil. The front surface of the target is exposed to a laser with an intensity of 3×10^{19} W/cm^2. At this laser intensity the interaction will produce relativistic electrons, which can heat the target at depth. Previous studies showed high-intensity short-pulse laser-driven hot-electron-induced shock-wave generation and propagation either with (i) low contrast intensity contrast (10^{-8} over 2.5 ns) pulses [11, 12] or with (ii) long pulses ($\sim$ 600 ps) [13] by monitoring the self-emission from the target rear. We probe the plasma at the rear of the target with a time delayed second harmonic (400 nm) probe, extracted from the main interaction laser pulse. Fast electrons travel at near light speed and ionize the target rear, causing probe absorption soon after pump irradiation. Interestingly, we see a shock-induced rise in the reflectivity at the rear of a 12 μm thick Al-foil only 30 ps after the interaction with the pump pulse. Here we explore the origins of this shock wave and show that it appears to form at depth within the target, driven by pressure gradients induced by hot electron driven prompt heating. This is interesting given that this shock wave is distinct from that formed in the low density plasma at the front surface which has been observed previously [6, 8].

Studying the hydrodynamics in a scenario such as this can give a number of insights. Firstly, as mentioned, it is important to understand the behaviour of the rear-surface of a solid target when the front-surface interacts with a high-intensity short-pulse laser due to the importance of the target rear for ion-acceleration applications.

The results of experiments of this type can, by informing modelling efforts, guide the design of ion-acceleration targets by supporting our understanding of the dynamics of the target rear-surface. Secondly, as will be shown, reproducing the experimental results using numerical simulations is dependent upon the electron transport and consequent heat deposition being modelled by a hybrid particle-in-cell code. As such we can use investigations of this type to help assess the extent to which electron transport and heating can be accurately modelled in relativistic laser-plasma interactions. Previous investigations [21] have shown the value of hydrodynamics data in supporting our understanding of relativistic laser-plasma-interaction driven electron generation, transport and heating.

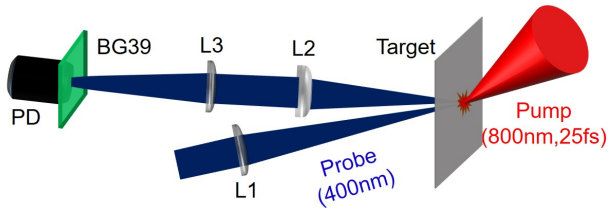

FIG. 1. (color). Schematic of the experimental setup: an intense laser pulse (pump) creates the plasma at the front of the target. A fraction of this optical pulse is split off, converted to its second harmonic (2ω, 400 nm) using a BaB_2O_4 crystal (BBO) and is then used as a probe. The temporal delay of the probe pulse with respect to the main interaction pulse is controlled precisely to capture the temporal evolution of the plasma with 100 femtosecond temporal resolution. L1, L2, L3 are achromatic lenses of focal lengths of 20, 15 and 20 cm respectively. BG 39 - bandpass filters, PD - a photo-diode.

EXPERIMENT

The experiment was performed with the 100 TW laser system at the Tata Institute of Fundamental Research, Mumbai. A p-polarized laser pulse of 25 femtosecond duration was focussed with an f/3 off-axis gold coated parabolic mirror to a 10 μm spot on the target at a 45^o angle of incidence, creating a laser intensity of 3×10^{19} W/cm^2. The laser contrast (picosecond pedestal/ peak intensity) was 10^{-10} ensuring minimal preplasma. Aluminium foils of 12 μm and 5.5 μm thickness were used as targets. The target was translated on a computer controlled X-Y stage so that the interaction laser pulse hit a fresh spot during each laser shot. A small fraction (5%) of the main interaction pulse was extracted with the help of a beam-splitter to generate the 2ω (400 nm) probe with a BBO crystal. The time delay between the main interaction laser pulse and the probe pulse was controlled (with precision of 7 fs) with the help of a computer controlled delay stage. The 2ω probe was focused to a 75 μm diameter spot to sample the rear plasma. The probe pulse was appropriately attenuated to ensure that it did not create plasma on its own (probe intensity $\sim 10^{10} Wcm^{-2}$). The differences with the earlier experiments [11, 12] are (i) the diagnostic we have employed, (ii) laser intensity, and (iii) laser pulse width and temporal contrast. The major advantage of using pump-probe technique is the temporal resolution of the measurement, $\sim$ 100 fs in present case, compared to 100 ps [11–13].

RESULTS AND DISCUSSION

Figure 2(a) shows the 2ω probe reflectivity from the rear of a 12 μm thick Al-foil target after a laser with an intensity of 3×10^{19} W/cm^2 has interacted with the front surface. The time t = 0 is defined as the instant at which the reflectivity of the probe beam starts decreasing due to the formation of a plasma layer caused by the fast electrons created at the target front. The rear-surface reflectivity falls to 30% within 20 ps of the arrival of the pump pulse at the front surface with a time constant τ_1 = 12.9 ps. There is a prominent rise in the reflectivity to 80% at $\sim$ 30 ps , followed by a decrease in the next 30 ps with a time constant τ_2 = 7.8 ps.

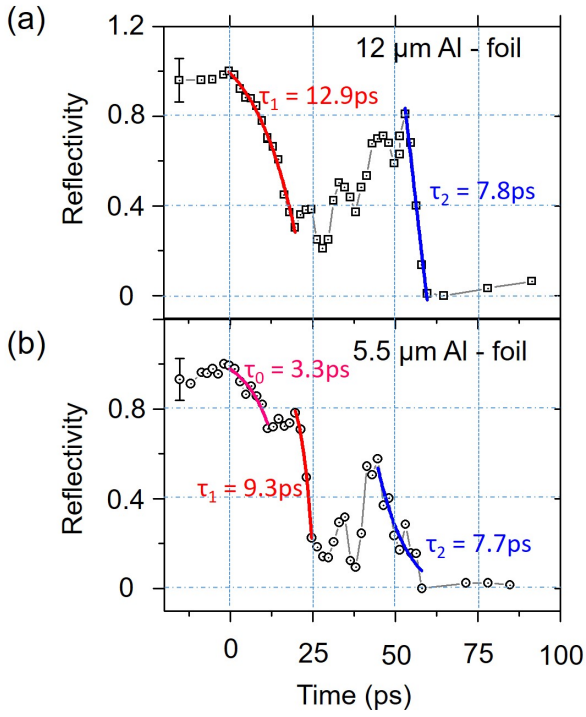

FIG. 2. (colour) Time resolved reflectivity at the rear surface of (a) a 12 μm and (b) a 5.5 μm thick Al-foil after a laser with an intensity of 3×10^{19} W/cm^2 has interacted with the front surface.

This initial fall in the probe reflectivity can be ex-

plained as follows: the main laser pulse creates a relativistic electron pulse which propagates through the target speed close to the speed of light in free space, reaching the rear surface of the 12 μm foil in less than a picosecond. It ionizes the foil leading to an expanding plasma that absorbs the probe pulse. The decay time can be explained by collisional absorption of the probe in this plasma, modelled by an exponential density profile $n_e = n_c \exp(-z/L)$. The rate of collisional absorption is proportional to $\exp(-t/\tau)$, where $\tau = 3c/8\nu_{ei}(n_c)L$, $\nu_{ei}(n_c)$ is the electron-ion collision frequency, c is the speed of light in free space and L is the length scale of the expanding plasma written as $L = c_s t$ at any instant of time, c_s being the expansion velocity of the critical surface inside plasma[2, 9]. For 400 nm probe the velocity of the critical density profile c_s can be measured using Doppler shift measurements [6–8]. The initial fall with a rate $\tau_1 = 12.9$ ps, agrees well with the collisional absorption model [9].

The subsequent rise in reflectivity can be explained by considering shock induced ionization and profile steepening. The shock reaches the target rear approximately 30 ps after the laser interaction at the target front. Here, the decay rate $\tau_2 = 7.8$ ps, which is faster than the initial decay $\tau_1 = 12.9$ ps. In order for a shock wave to propagate through a 12 μm foil in 30 ps, it would need to travel at a mean velocity of 4×10^7 cm/s, however such a suggestion would seem inconsistent with the measurements made on a thinner foil, as shown below.

The reflectivity at the rear surface of a 5.5 μm Al-foil target under similar experimental conditions was also measured. The results are shown in Fig. 2(b). We see, three distinct decreases in the reflectivity with different decay rates. Initially the reflectivity falls to 70% within 10 ps with $\tau_0 = 3.3$ ps. The reflectivity then stays nearly constant for a few picosecond before falling further to 20% with a time constant $\tau_1 = 9.3$ ps. There is a prominent rise in the reflectivity to 60% at $\sim$ 30 ps, and a decrease in the next 35 ps at a rate given by $\tau_2 = 7.7$ ps. The dynamics here appears somewhat more complex than in the case of the 12 μm foil, though the behaviour between 30 and 65 ps appears quite similar in both cases. Comparison of these two cases is interesting since it is not physically reasonable that a shock wave could propagate from the front surface in essentially the same time in both targets, given that they are of markedly different thicknesses, and have both been exposed to the same laser pulse. Even if the small increase in the reflectivity around 22 ps in the 5.5 μm foil case is taken as the shock arrival time at the rear-surface, it is still quite inconsistent with such a picture given that an unsupported shock wave would slow down considerably as it propagated through such a target. A shock that reached the rear surface of a 5.5 μm thick target in 22 ps would be expected to take significantly more than twice this time to reach the rear of a 12 μm thick foil. This expectation is further supported given the relatively small focal spot of the pump laser, which would promote substantial lateral energy loss from the central region of the shock if it propagated a distance comparable to the 10 μm laser-spot diameter on the front surface. For this reason we decided to model the propagation dynamics to better understand the behaviour of the two targets.

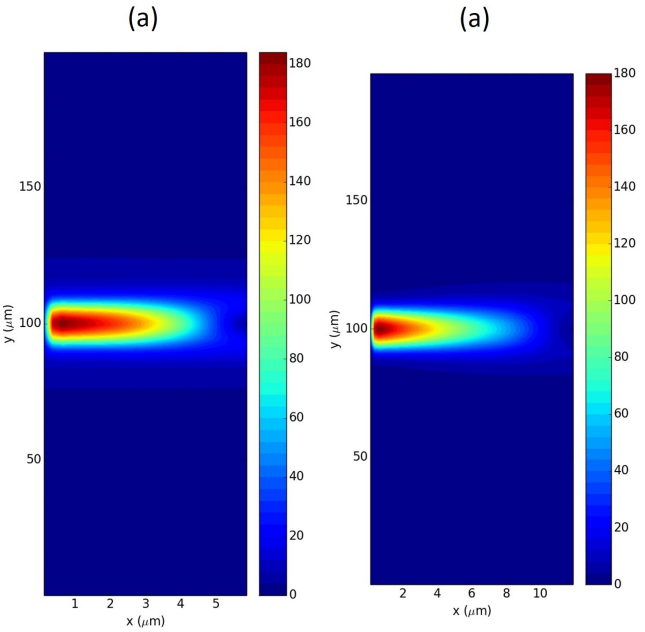

FIG. 3. (colour) ZEPHYROS simulations of the heating induced by the interaction with the laser for the (a) 5.5 μm Al-foil and the (b) 12 μm Al-foil targets.

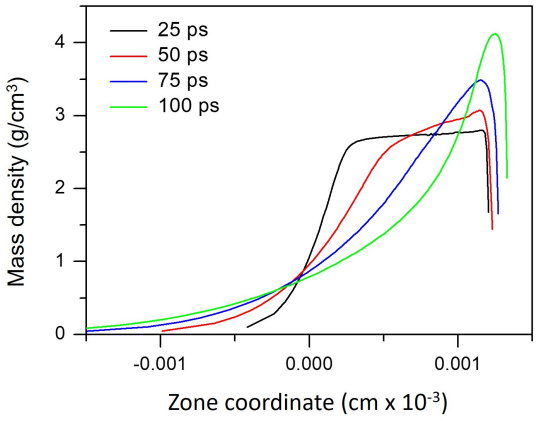

FIG. 4. (colour) Sequence of snapshots from the HYADES simulation showing the evolution of the shock wave driven by the temperature profile input from ZEPHYROS in the 12μm thick target.

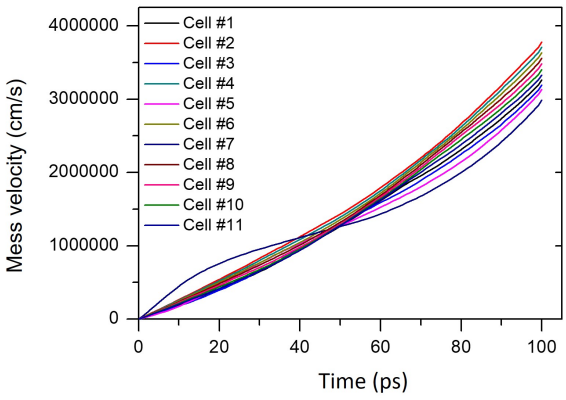

FIG. 5. (colour) Motion of the rearmost ten lagrangian fluid cells in the HYADES simulation of the 12 μm thick target.

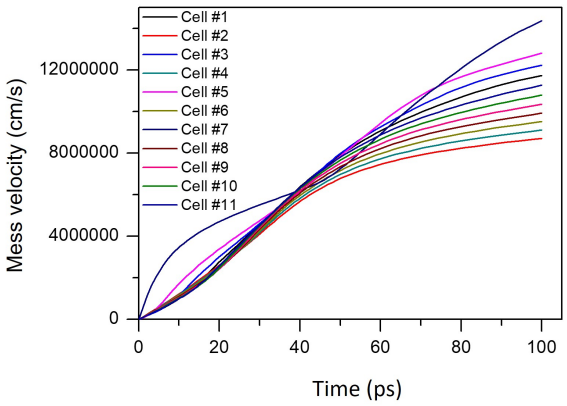

FIG. 7. (colour) Motion of the rearmost ten lagrangian fluid cells in the HYADES simulation of the 5.5 μm thick target.

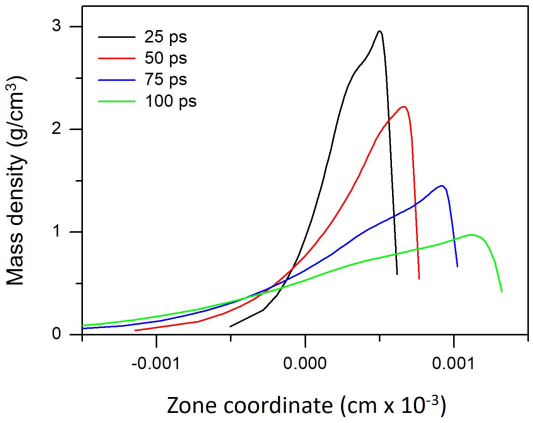

FIG. 6. (colour) Sequence of snapshots from the HYADES simulation showing the evolution of the shock wave driven by the temperature profile input from ZEPHYROS in the 5.5μm thick target.

NUMERICAL SIMULATIONS

The heating in both the 5.5 μm and 12 μm Al-foil targets was modelled separately using the Hybrid particle-in-cell simulation code ZEPHYROS [18, 19]. ZEPHYROS was run with 2×10^8 particles and a mean particle density of 25 particles per cell. Radiation-hydrodynamics simulations based on the heating profile produced by ZEPHYROS were then performed using HYADES [20]. The HYADES calculations employed SESAME equation of state data for Aluminium, a multi-group diffusion model for thermal radiation, and a flux-limited diffusion model for electron conduction. Figure 3 shows the temperatures predicted by ZEPHYROS to be induced in the target due to interaction with the laser.

The HYADES calculations show shock break-out in both targets driven by the heating induced by the short pulse. A time sequence of results for the 12 μm Al-foil target are shown in Fig. 4 with the trajectories of the rearmost Lagrangian fluid elements being shown in Fig. 5. Following a brief period of free surface expansion, driven by the hot electron heating, there is compression and acceleration of the rear of the target between around 30 and 60 ps driven by the passage of the shock wave. A time sequence of results for the 5.5 μm Al-foil target is shown in Fig. 6 with the trajectories of the rearmost Lagrangian fluid elements being shown in Fig. 7. These results show shock compression and acceleration of the 5.5 μm target rear between 20 and 45ps. Although these simulations do not include two-dimensional effects, it is clear that the shock wave here is only propagating for a fraction of the width of the target (approximately one micron) prior to break-out, meaning that the shock propagation at early time can be treated reasonably with a one dimensional code. This is interesting in the light of previous studies examining shock wave propagation at the front surface of targets driven by ultra-short high-intensity laser pulses, since it demonstrates that this shock emerging from the rear of the target a few tens of picoseconds after the laser-target interaction is distinct from that being driven in the low-density plasma at the front surface [6, 8]. Rather than a single shock wave being launched at the front of the target, and propagating through to the rear, the shock wave that is observed at the rear of the target is being driven by the prompt heating at depth in the initially cold bulk target material. This prompt heating causes a shock wave to form close to the rear surface of the target for targets of the thicknesses utilised in this study. It is this shock wave, formed at depth within the target, that is observed in the experiments reported upon here. It should further be noted that in the case of substantially higher laser energies, or thinner targets, the center of the target can be

volume heated such that it simply rarefies without the formation of a rearward propagating shock at the back surface; such dynamics have been observed [22]. Another point of interest here is that, in the HYADES simulation the thinner target is more effectively accelerated by the driver than its thicker counterpart, as shown by motion of the peak density region in the x-direction in Fig. 6. The results suggest that the reflectivity peak observed in the experiment around 25 ps represents the time of shock breakout from the denser plasma, whilst the later peak with somewhat lower reflectivity around 50 ps may be due to re-compression of the lower-density plasma by the accelerated plasma layer.

CONCLUSIONS

We have studied the plasma dynamics at the rear of thin Al-foil targets at relativistic laser intensity using pump-probe reflectivity. Experimental results show that for 5.5 and 12 μm thick Al-foil targets, there is a rise in the reflectivity (for a 400 nm probe pulse) a few tens of picoseconds after the main laser pulse interaction. This rise in the reflectivity can be explained by considering shock propagation through the plasma at the target rear surface. Simulations reveal that this shock wave is launched from deep within the target by the fast electron driven heating of the dense plasma, rather than propagating all the way through the target from the front surface. Our ability to reproduce the timing of the shock break-out in the two targets support the use of ZEPHYROS in modelling laser-plasma interactions in this regime, however there are clear limitations in the present modelling effort, both in terms of the use of 1D- rather than 2-D hydrodynamic modelling, and due to the limited extent to which data is passed between the PIC and hydrodynamic modelling routines.

Acknowledgements:
G.R.K. acknowledges partial support from J.C. Bose Fellowship grant JCB-37/2010 of the Department of Science and technology, Ministry of Science and Technology, Government of India. G.R.K and J.P thank the Newton-Bhabha UK-India programme for facilitating this collaboration. M.S. thanks Sachin Prabhakar for his help.

* grk@tifr.res.in

[1] P. Gibbon, Short Pulse Laser Interactions with Matter (Imperial College Press, 2005).
[2] W. L. Kruer, The Physics of Laser Plasma Interactions (Westview Press, Boulder, Colorado, 2003).
[3] R. P. Drake, High-Energy-Density Physics-Fundamentals, Inertial Fusion and Experimental Astrophysics (Springer, Berlin, Heidelberg) (2006).
[4] M. Tabak, J. Hammer, M. E. Glinsky, W. L. Kruer, S. C. Wilks, J. Woodworth, E. Michael Campbell, M. D. Perry, and R. J. Mason, Phys. Plasmas **1**, 1626 (1994).
[5] L. O. Silva, M. Marti, J. R. Davies, and R. A. Fonseca, Phys. Rev. Lett. **92,** 1 (2004).
[6] S. Mondal, A. D. Lad, S. Ahmed, V. Narayanan, J. Pasley, P. P. Rajeev, A. P. L. Robinson, and G. R. Kumar, Phys. Rev. Lett. **105,** 105002 (2010).
[7] K. Jana, D. R. Blackman, M. Shaikh, A. D. Lad, D. Sarkar, I. Dey, A. P. L. Robinson, J. Pasley, and G. R. Kumar, Phys. Plasmas **25,** 013102 (2018).
[8] A. Adak, D. R. Blackman, G. Chatterjee, P. K. Singh, A. D. Lad, P. Brijesh, A. P. L. Robinson, J. Pasley, and G. Ravindra Kumar, Phys. Plasmas **21,** 062704 (2014).
[9] P. K. Singh, G. Chatterjee, A. Adak, A. D. Lad, P. Brijesh, and G. R.Kumar, Opt. Express. **22,** 19 (2014).
[10] A. Adak, A. P. L. Robinson, P. K. Singh, G. Chatterjee, A. D. Lad, J. Pasley, and G. R. Kumar, Phys. Rev. Lett. **114,** 115001 (2015).
[11] K. Jakubowska, D. Batani, J.-F. Feugeas, P. Forestier-Colleoni, S. Hulin, P. Nicolai, J. J. Santos, A. Flacco, B. Vauzour, and V. Malka, Euro. Phys. Lett. **119,** 35001 (2017).
[12] J. J. Santos *et al.*, New J. Phys. **19,** 103005 (2017).
[13] A. Benuzzi, M. Koenig, B. Faral, J. Krishnan, F. Pisani, D. Batani, S. Bossi, D. Beretta, T. Hall, S. Ellwi, S. Huller, J. Honrubia, and N. Grandjouani, Phys. Plasmas, **5,** 2410-2420 (1998).
[14] J. J. Honrubia, R. Dezulia, D. Batani, S. Bossi, M. Koenig, A. Benuzzi and N. Grandjouan, Laser Particle Beams, **16,** 13-20 (1998).
[15] P. Antici, J. Fuchs, M. Borghesi, L. Gremillet, T. Grismayer, Y. Sentoku, E. d'Humières, C. A. Cecchetti, A. Mančić, A. C. Pipahl, T. Toncian, O. Willi, P. Mora, and P. Audebert, Phys. Rev. Lett. **101,** 105004 (2008).
[16] P. Antici, S. N. Chen, L. Gremillet, T. Grismayer, P. Mora, P. Audebert, and J. Fuchs, Rev. Sci. Instrum **81,** 113302 (2010).
[17] J. S. Green, C. D. Murphy, N. Booth,a R. J. Dance, R.J. Gray, D.A. MacLellan, P. McKenna, D. Rusbya and L. Wilson, JINST **9,** P03003 (2014).
[18] S. Kar, A.P.L. Robinson, D.C. Carroll, O. Lundh, K. Markey, P. McKenna, P. Norreys, and M. Zepf, Phys. Rev. Lett. **102,** 055001 (2009).
[19] B. Ramakrishna, S. Kar, A. P. L. Robinson, D. J. Adams, K. Markey, M. N. Quinn, X. H. Yuan, P. McKenna, K. L. Lancaster, J. S. Green, R. H. H. Scott, P. A. Norreys, J. Schreiber, and M. Zepf, Phys. Rev. Lett. **105,** 135001 (2010).
[20] HYADES is a commercial product of Cascade Applied Sciences, email: larsen@casinc.com
[21] K. L. Lancaster, J. Pasley, J. S. Green, D. Batani, S. Baton, R. G. Evans, L. Gizzi, R. Heathcote, C. Hernandez Gomez, M. Koenig, P. Koester, A. Morace, I. Musgrave, P. A. Norreys1, F. Perez, J. N. Waugh, and N. C. Woolsey, Phys. Plasmas. **16,** 056707 (2009).
[22] K. L. Lancaster, A. P. L. Robinson, J. Pasley, P. Hakel, T. Ma, K. Highbarger, F. N. Beg, S. N. Chen, R. L. Daskalova, R. R. Freeman *et al.*, Phys. Plasmas. **24,** 083115 (2017).